PHYSICAL REVIEW D **90,** 022004 (2014)

Pioneer 10 and 11 orbit determination analysis shows no discrepancy with Newton-Einstein laws of gravity

D. Modenini* and P. Tortora†

Department of Industrial Engineering, University of Bologna, Via Fontanelle 40, I-47121 Forlì, Italy

(Received 21 November 2013; revised manuscript received 30 April 2014; published 22 July 2014)

The present work describes our investigation of the navigation anomaly of the Pioneer 10 and 11 probes which became known as the Pioneer Anomaly. It appeared as a linear drift in the Doppler data received by the spacecraft, which has been ascribed to an approximately constant Sunward acceleration of about 8.5×10^{-13} km/s^2. Since then, the existence of the anomaly has been confirmed independently by several groups and a large effort was devoted to find its origin. Recently, different analyses were published where the authors claimed the acceleration due to anisotropic thermal emission to be the most likely cause of the unexplained acceleration. Here we report the methodology and the results of an independent study carried out in the last years, aimed at supporting the thermal origin of the anomaly. This work consists of two main parts: thermal modeling of the spacecraft throughout its trajectory, and orbit determination analysis. Based on existing documentation and published telemetry data, we built a thermal finite element model of the spacecraft, whose complexity has been constrained to a degree allowing for sensitivity analysis, leading to the computation of its formal uncertainty. The trajectory analysis and orbit determination were carried out using NASA/JPL's Orbit Determination Program, and our results show that orbital solutions are achieved that do not require the addition of any "unknown" acceleration other than that of thermal origin.

DOI: 10.1103/PhysRevD.90.022004 PACS numbers: 04.80.-y, 95.10.Eg

I. INTRODUCTION

The so-called Pioneer Anomaly is an anomalous blueshift in Pioneer 10 and 11 radiometric tracking data, which has been interpreted as a constant Sunward acceleration pulling the probes back during their journey towards and beyond the bounds of the Solar System. Since its discovery [1], the existence of the anomaly has been confirmed independently by several authors; see e.g. Refs. [2–4]. Since no conventional effects (e.g. unaccounted on-board or environmental systematic effects) were found to be completely satisfactory, some authors have been suggesting more unconventional causes: these include modifications of the gravity law at scales of the Solar System size, or even the presence of dark matter; see for example Refs. [5] or [6]. The Pioneer Anomaly is considered by many authors as a deviation from Newton-Einstein gravity law.

Here we show that no anomalous acceleration acted on the spacecraft, and its evidence reported in many papers is due to a lack in modeling Pioneer spacecraft dynamics: in particular, a model of recoil force due to anisotropic thermal radiation emitted must be added.

In recent years, several authors suggested the recoil force due to anisotropic infrared emission as a possible on-board effect for explaining the anomaly. Even if in their early investigation [1] Anderson *et al.* discarded the thermal recoil force (TRF) as a source of a significant bias acceleration, its impact was reconsidered soon after by Katz in his comment [7]. The author stated that the recoil due to the fraction of thermal power radiated by the radioisotope thermoelectric generators (RTGs) being scattered from the back of the spacecraft antenna, together with the on-board dissipated electrical power radiated from the back of the spacecraft were compatible with the reported anomalous acceleration. This conclusion, however, was disputed by Anderson *et al.* in their response [8]. While both the above contributions were mainly semiquantitative, only more recently has the study of the TRF acting on Pioneer spacecraft been the subject of deeper analyses, such as the ones in Refs. [9–13]. In particular, the authors of Ref. [11] started from the realization that, if a force of thermal origin really acted on the probes, it should have exhibited a time decrease following the nuclear decay of plutonium (the source of power for the probes) to show that the observed drift in Doppler residuals is compatible with accelerations varying on the same time scale. In Ref. [12], the authors present a thermal model of the Pioneer spacecraft based on the Phong shading technique, while the authors of Ref. [13] develop a detailed finite element model which estimates the radiation pressure through a ray-tracing algorithm capable of handling reabsorption and multiple reflections. Both works, even if starting from quite different modeling strategies, obtained estimates of the thermal recoil acceleration which are compatible with the reported anomalous one. The assessment of the time evolution of the thermal acceleration throughout the trajectory was performed in Ref. [12] by fitting to an exponential decay model the mean values and the upper and lower bounds

*dario.modenini@unibo.it
†paolo.tortora@unibo.it

based on 95% probability levels, obtained from Monte Carlo simulations performed at three selected trajectory points. In Ref. [13], simulations were performed at 1 year temporal resolution along the trajectory of Pioneer 10, and an overall worst-case accuracy of 11.5% was obtained from a sensitivity analysis of the model. However, in both Refs. [12,13], no Doppler tracking data analysis was performed. In Ref. [14], Turyshev *et al.*, by combining the output of a sophisticated thermal model of the spacecraft with the analysis of Pioneer 10 tracking data, concluded that the thermal recoil force due to the anisotropic infrared emission is the cause of the drift of the Doppler residuals, which gave rise to the so-called "Pioneer Anomaly."

In this context, the investigation presented herein further supports and strengthens the claim of the thermal origin of the anomalous acceleration by focusing on the following aspects, which were not examined in depth in previously published papers:

1. Development of a thermal model having, as main driver, its consistent integration within the orbit determination process.
2. A comprehensive analysis of both Pioneer 10 and Pioneer 11 tracking data with the same level of detail.
3. Enhancement of the robustness of the main conclusions by adding further orbit determination runs which explicitly exclude the presence of a residual unmodeled acceleration besides the thermal recoil one.

With the above goals in mind, we performed a thermal analysis by developing a finite element model of the probes, whose complexity was constrained to a degree allowing for a Monte Carlo sensitivity analysis. The output of the thermal model was then fitted as a function of time depending on a finite set of coefficients, whose uncertainty is given in terms of a covariance matrix to be incorporated into the orbit determination filter. This approach is believed to provide a consistent integration of the two aspects of our investigation, namely the spacecraft thermal modeling and the radio tracking data processing. An analysis of the most complete data sets of both Pioneer 10 and Pioneer 11 was then performed, with the thermal recoil force resulting from our thermal model included (along with its uncertainty) as an additional dynamical model. This allowed us to determine if our estimated thermal recoil force yielded satisfactory, zero-drift residuals, orbital solutions. We deem this approach to be more rigorous, from a trajectory determination point of view, than a simple order-of-magnitude comparison between the anomalous acceleration, as derived from previous orbital solutions, and the recoil acceleration resulting from the thermal analysis. Moreover, this orbit determination setup allowed us to go further in our analysis and to answer the question of whether the presence of any additional unmodeled acceleration, other than that of thermal origin, could be supported by the Doppler data. Finally, to gather confidence in our results, we compared the outcome of two different implementations of the orbit determination filter, the standard single-arc and the multi-arc techniques, the latter being more suited when very long trajectory arcs are under consideration.

The paper is organized as follows: Section II discusses the thermal model of the Pioneer spacecraft, presenting the fundamental theoretical aspects and the modeling steps; focus is placed on the issues related to the integration of the results into the Orbit Determination Program (ODP). In Sec. III, the basics of the orbit determination theory are covered; the implementation details (filtering techniques, data editing) are deeply discussed. In Sec. IV, the results of the analyses of Pioneer 10 and 11 Doppler tracking data are presented and examined. Finally, in Sec. V, conclusions drawn from the overall investigation are discussed and summarized.

II. PIONEER THERMAL MODEL

The Pioneer spacecraft are depicted in Figs. 1 and 2. The main sources of power on board Pioneer spacecraft are four radioisotope thermoelectric generators (RTGs). The thermal power generated by the RTGs was nearly 2580 W at launch; its amount is expected to decay during the mission following the plutonium half-life time (87.7 years). A fraction of this thermal power (≈ 160 W at launch) is converted into electrical power, which supplies the various instrumentation placed on board. In particular, part of it is transmitted towards the Earth as a radio beam, while the remaining part is converted into heat by the Joule effect: this waste heat is radiated into space through the main compartment external surfaces and a louver system which ensures thermal control of the spacecraft. In other words, all power generated inside the Pioneer spacecraft is expelled in

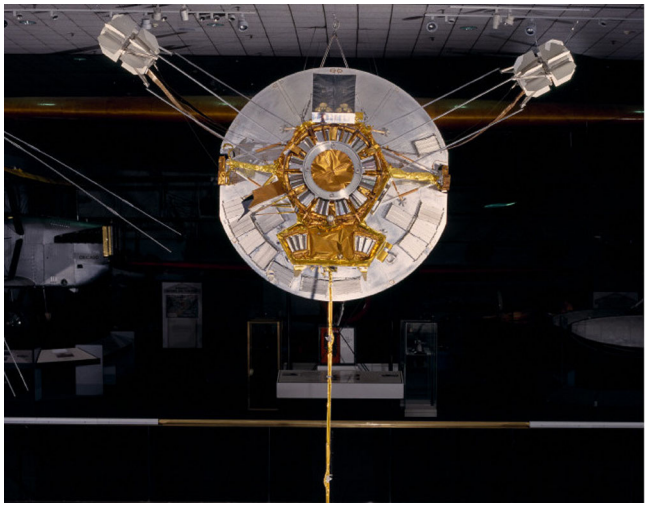

FIG. 1 (color online). Prototype of Pioneer 10 displayed in the Smithsonian National Air and Space Museum.

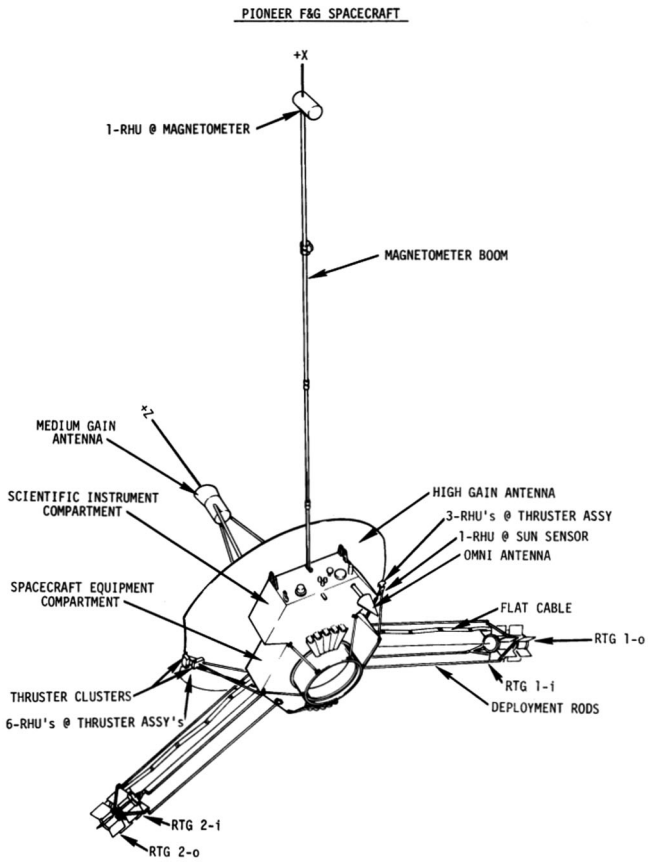

FIG. 2. Pioneer F/G spacecraft main components from Ref. [15].

the form of electromagnetic radiation (either IR or radio beam), which carries momentum with it. If the radiation pattern is anisotropic, the momentum exchange between the spacecraft and the emitted radiation results in a recoil force which affects the trajectory of the probe.

The component of the recoil force in a certain direction equals the unbalanced power output in the same direction divided by the speed of light. Therefore, a simple order-of-magnitude analysis tells us that, the mass of the spacecraft being ≈ 250 kg, only a small fraction of the total available power, $\simeq 60$ W, directionally radiated away from the Sun would cause an acceleration equal to the anomaly. It is hence clear that recoil force due to radiation should be properly estimated and included in the orbit determination process.

By inspection of the macroscopic configuration of Pioneer geometry as visible in Figs. 1 and 2, one can identify at least two mechanisms which are likely to be responsible for a certain degree of anisotropy in radiation emission:

1. Heat from RTGs rejected by the highly reflective back side of the high-gain antenna.
2. Electrical heat dissipated inside the bus having a preferable escape direction through the louver system.

Both these contributions are mostly directed as the anomaly, but while the first depends on thermal power, the second depends on electrical power. There is actually another source of thermal energy on board other than the RTGs: nine radioisotope heater units (RHUs) generating 1 W each, and deputed to heat up thruster cluster assemblies. However, according to Turyshev [16], their geometric configuration and location are such to prevent them from contributing substantially to anisotropic radiation. In earlier papers [17], it was pointed out that the secular time evolution of the RTGs' power is quite in contrast with the evidence of a constant anomaly, even if Markwardt's analysis [2] of the set of data between 1987 and 1998 claims that the Doppler shift is compatible with a jerk term of a time scale similar to the decay of plutonium. More recently, Turyshev [11] arrived at a similar conclusion using extended data sets of both Pioneer 10 and 11 and testing for a linear and an exponential time decay of the anomaly. In the present work, we also explore the temporal variation of the recoil force of thermal origin; however, we do not restrict ourselves to the case of a monotonic decrease, as could be expected for an effect driven only by the available on-board power. The spacecraft's infrared emission depends on the total energy input to the spacecraft which, besides the RTGs' power, also includes irradiation from the Sun. The solar flux effect on spacecraft dynamics is twofold. On one side there is the solar radiation pressure, which is commonly accounted for during trajectory integration. The ODP implements a model to estimate the momentum exchange between the solar flux and the spacecraft components. On the other hand, the solar flux induces a temperature increase on the illuminated surfaces due to the fraction of radiation which is adsorbed. For the Pioneers, this is the case, especially for the high-gain antenna, which is constantly pointed towards Earth and also fully illuminated by the Sun, at least at sufficiently large heliocentric distances. The parabolic dish is basically a thin surface with highly different emittance on the two sides: the back side of the antenna is highly reflective with a low emittance, while the white painted front side is highly emittive (see Table I). Therefore, the solar power is almost entirely dissipated by the Earth-pointing antenna face, resulting in a recoil force antiparallel to the contribution of the internally generated power, hence subtracting from its amount. The subtracting term due to the solar flux decreases with time as well because of the probes receding from the Sun, such that, as a result, our thermal model reconstructs a recoil force which does not decrease with time monotonically.

A. Thermal radiation theory for spacecraft modeling

The thermal model of the spacecraft includes a simplified discretized geometry of the probe, which has been developed based on the existing design documentation. The thermal state has been reconstructed from published

TABLE I. Thermo-optical properties of main Pioneer surfaces relevant to thermal model.

Element	Material	Surface coating	ϵ	α
HGA front side	Al 6061	DC92-007 white paint	0.85	0.21 (0.50)
HGA back side	Al 6061	white paint	0.04	0.17
RTG body	HM31A-F Mg	white paint	0.82	0.21 (0.50)
RTG fins	HM21A-T8 Mg	white paint	0.82	0.20 (0.50)
S/C MLI	Al 6061	aluminized Mylar/Kapton	0.69 (0.0085)	0.20/0.46
Louvers	Al 6061	bare	variable	N/A
ALR interior	Al 6061	black paint	0.84	0.95
ALR exterior	Al 6061	bare	0.10	0.24

recovered telemetry data [16] which consist of measurements of power generation/consumption and temperature readings from several sensors located on the RTG fins, the body panels, and inside the payload bay. However, while the energy input has been used quantitatively, the temperature information has been used only for a qualitative comparison with the thermal model predictions.

To determine the amount of radiation emitted by the spacecraft into space, the exchange of thermal energy between the different surfaces is required. The mathematical details behind this computation are of no interest here, and only the relevant modeling steps are presented. The process involves computation of the radiation balance on each element between emitted, adsorbed and reflected radiation, and of the so-called view factors between the discretized surface elements. The former can be computed by following the well-known Stephan-Boltzmann law:

$$q_{\mathrm{rad}} = \sigma \epsilon T^4, \tag{1}$$

where σ is the Stephan-Boltzmann constant, equal to 5.67×10^{-8} $\mathrm{W}/(\mathrm{m}^2\,\mathrm{K}^4)$, ε is the surface total hemispherical [18] emittance, and T is the absolute temperature. When radiation impinges over an opaque surface, Eq. (1) should be modified to account for the reflected and absorbed radiation such that the radiation energy balance can be expressed as follows:

$$q_{\mathrm{rad}} = J - H = (1-\varepsilon)H + \varepsilon\sigma T^4 - H = \varepsilon(\sigma T^4 - H). \tag{2}$$

In Eq. (2), J denotes the surface radiosity—i.e., the total heat flux leaving the surface due to emission and reflection—and H denotes the surface irradiation—that is, the total incoming heat flux [19]. Moreover, the assumptions of gray and diffuse emitting/reflecting surfaces have been retained (so-called Lambertian radiators [20]). The view factors provide a measure of the amount of the total radiation which, emitted by a surface, hits another surface after mutual shadowing. To compute them, one needs to know, in addition to the relative orientation between the surfaces, also the directional dependency of the emitted radiation. Under these hypotheses, the radiation pressure acting on an isolated flat surface element of area dA due to emitted radiation is given by the following expression:

$$p_{\mathrm{rad}} = \frac{2}{3c}\sigma\varepsilon T^4, \tag{3}$$

where c is the speed of light. The force due to such pressure acts in the surface-normal direction.

Radiation pressure can be generalized to account for absorption and reflection, such that a radiation recoil force can be computed at each surface element to be then integrated over the entire spacecraft surface. An alternative approach used in the present work consists of surrounding the spacecraft with a sphere acting as a control volume. This control volume is modeled as a passive blackbody—that is, a body at a constant temperature of 0 K and emittance of 1, such that it absorbs all the incident radiation without emitting or reflecting anything: The net radiation escaping out of the spacecraft system and detected by the control volume is the only contribution to the recoil force, since the contribution due to radiation intercepted (absorbed) by spacecraft components cancels out the pressure acting on the surfaces emitting such radiation. Conservation of energy requires that volumetric (Q) and surface ($\vec{q}$) heat sources input to the spacecraft balance the net radiation emitted by the spacecraft itself and impinging on the control volume (CV):

$$\iiint_{V_{\mathrm{Pio}}} Q dV + \iint_{S_{\mathrm{Pio}}} \vec{q}_{\mathrm{Sun}} \cdot \vec{n} dS = \iint_{S_{\mathrm{Pio}}} (J-H) dS = \iint_{CV} H dS. \tag{4}$$

This equation has been used to check the consistency of the implemented thermal model.

B. Spacecraft numerical model

The geometric model created for the Pioneers includes only the major spacecraft components, namely the high-gain antenna, the RTGs, the adaptor launch ring (ALR), and the spacecraft compartment bus plus the louver radiators. The energy input to the system consists of three volumetric heat sources, two placed inside the RTGs and one placed inside the spacecraft body, plus a surface heat flux to mimic the solar radiation impinging on the concave side of the high-gain antenna and on the RTGs (this last contribution is, however, negligible when compared to the thermal power inside RTGs), which are the only parts actually

exposed to it during the interplanetary cruise. As a baseline case study, we have assumed that, with the total amount of power being known from telemetry and the volume of the components where the heat sources are placed, the distribution of such sources is uniform within each component. This is, of course, a simplification, especially for the electrical power inside the bus, since the presence of several instrumentation components makes the produced heat more likely to be concentrated in some regions. The temperature readings from the six sensors placed on the bus platform indicate temperature differences of up to 30° C among the different locations. The impact of such temperature differences on the computed radiation pattern has been addressed by performing a set of Monte Carlo simulations, resulting in a relatively limited scatter of the recoil force, as will be detailed in Sec. II C.

The thermo-optical properties of surface materials were retrieved mainly from Ref. [15], and the relevant ones are reported in Table I. There are some minor differences between the values reported in Ref. [15] and those actually used in the present study, and these are reported within round brackets. In particular, the nominal values of solar absorptance are beginning-of-life values, which are likely to vary during cruise as an effect of surface degradation due to exposure to UV radiation and charged or contaminating particles. The generalized result is an increase in the solar absorptance [21]. In Ref. [22], white paint absorptance is reported to increase from ≈ 0.20 up to ≈ 0.60 in a few years of the mission. Moreover, for the multilayer insulation (MLI), the design documentation reports the emittance of the external layer, 0.70, while, as pointed out in Ref. [9], an effective emittance should be used instead which lies in the range $0.007 \div 0.01$.

The presence of the louver system has been simulated by specifying a variable emittance over a region surrounding the ALR, which is a function of the temperature and spatial coordinates. Therefore, no detailed geometric components for blades, springs and platform have been used. It has been rather preferred to use as driving information the wattage dissipated by the louver system as a whole, across its operating temperature range (from 4° C to 32° C). Such quantities can be retrieved from the plots in Fig. 3, which were taken from Ref. [16]: the first reproduces the power radiated by each two-blade and three-blade assembly, while the second provides heat loss from the louver structure. Based on these diagrams, the following empirical function for emittance variation was implemented in the thermal model:

$$\varepsilon = 0.01 + 0.58 - \frac{0.38}{1 + \exp(0.35(T - 288))} e^{-10|x^2+y^2-0.4^2|}. \tag{5}$$

Where x and y represent in-plane coordinates orthogonal to the focal axis of the HGA. The function used in Eq. (5), an

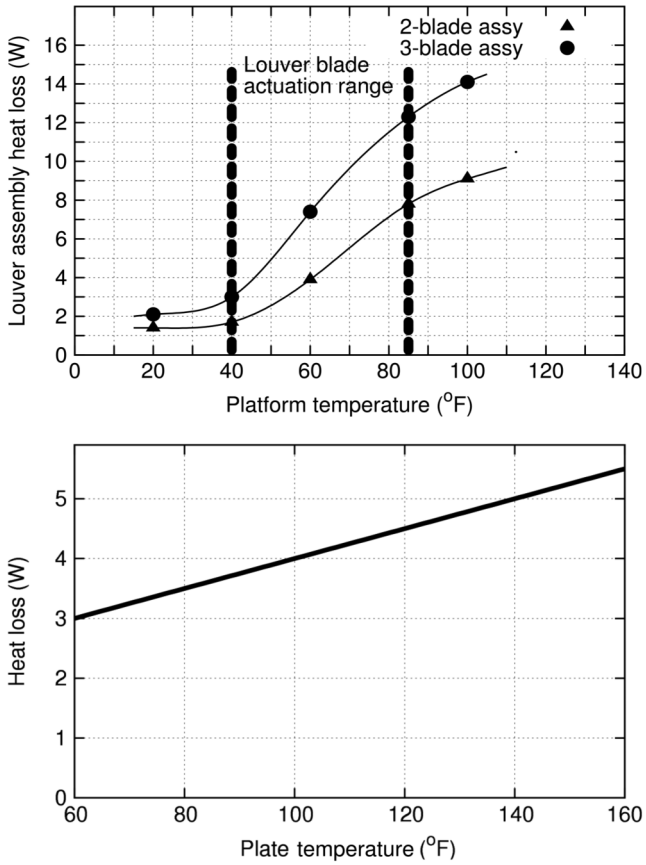

FIG. 3. Heat dissipated by louvers, taken from Ref. [16].

S-shaped exponential for dependence upon temperature, Gaussian bell-shaped for dependence upon spatial coordinates, was arbitrarily selected just to avoid sharp discontinuities. Outside the temperature actuation range, the emittance is kept constant, which seems a reasonable assumption. The numerical coefficients in Eq. (5) were tuned in order to match the value of the radiated power extrapolated from the top panel in Fig. 3 at four measured temperatures. From the Stephan-Boltzmann law, it follows that prescribing the radiated power at a certain temperature is equivalent to prescribing the area integral of the emittance, $\int \varepsilon dA$: the computed values are collected in Table II.

Equation (5) indicates that the louvers' equivalent emittance equals 0.21 in fully closed configuration and 0.59 in fully open condition. These numbers are somehow in disagreement with data found in Ref. [15] itself, which

TABLE II. Heat loss from louvers and related emittance surface integrals.

T platform [K]	Louver heat loss [W]	$\int \varepsilon dA$ [m^2]
266	20	0.07
278	30	0.09
288.7	64	0.16
303	124	0.26

reports $\varepsilon = 0.04$ for the blades and 0.82 for the radiating platform underneath. In this respect, we explicitly note that the surface integral of Eq. (5) is highly dependent on the type of mesh used in the numerical model; in other words, the relevant physical data is the value of $\int \varepsilon dA$, while the resulting emittance is intimately related to, and a consequence of, the actual discretized geometry. The inconsistency is therefore only apparent. Once again, it is noted that the driving criterion is the preservation of the total power emitted by the louvers according to the design documentation, rather than matching the detailed geometry, surface area or emittance separately. It is certainly true that the radiated power can be indirectly inferred by the temperature, area and emittance of a surface, but, on the other hand, when a direct measure of the radiated power is available, as for the louvers, it seems reasonable to prefer this source of information.

The output of the full thermal model is the amount of radiation which, after mutual reflection among surfaces, escapes the spacecraft system to hit the control volume. The integral of the radiation flux impinging the control volume and projected along the high-gain antenna axis direction provides the magnitude of the anisotropic emitted power.

C. Thermal simulation output sensitivity and covariance analyses

To assess the sensitivity of the thermal model to parameters which are not exactly known, and as a method to provide confidence bounds for the results, a series of Monte Carlo simulations and a covariance analysis were set up. The objective of this process is to obtain a fit of the recoil force as a function of thermal power P_{th}, electrical power P_{el}, and solar flux Φ_S (known input parameters), while a number of other parameters are allowed to vary over the simulations over a certain space (uncertain parameter space). These include surface emittance and absorptance, and power distribution within volumes. In particular, allowing for a nonuniform power distribution inside a component is a way to mimic, within the frame of our thermal model, the presence of a spatial variation in the temperature over the bus and the RTGs, which was indeed highlighted by the Pioneer telemetry temperature data. The volumetric heat source distribution functions inside the RTGs (Q_{th}) and the spacecraft bus (Q_{el}) [23] were arbitrarily assumed as being sinusoids of the spatial coordinates. The amplitudes and phases of such sinusoids belong to the uncertain parameter space [24].

The solar absorptances of the high-gain antenna and of RTGs were varied according to

$$\alpha_i = \bar{\alpha}_i + d\alpha_i, \tag{6}$$

where $\bar{\alpha}_i$ is the nominal absorptance set equal to 0.5 and $d\alpha_S$ is sampled drawn from uniform distributions in the open interval $(-0.1, 0.1)$. The uncertainty in surface emittance coefficients was set to 15% of the nominal value

$$\varepsilon = \bar{\varepsilon}_i + d\varepsilon_i, \tag{7}$$

where $\bar{\varepsilon}$ is the nominal emittance of the ith modeled surface, and the values for $d\varepsilon_i$ are sampled from a uniform distribution inside the interval $(-0.15\overline{\varepsilon_i}, 0.15\overline{\varepsilon_i})$.

Numerical consistency of the method has been checked according to Eq. (4). Our results indicate that while the first equality is always satisfied (difference below 10^{-7} W), the second equality gives residuals in the order of 2 to 3 W, which reflects in about 0.1% of the total input power. If one assumes this energy unbalance having no preferential direction, the discrepancy per unit solid angle is $3\ \mathrm{W}/4\pi \simeq 0.23$ W. This value can be assumed as a figure of merit of the numerical error affecting the computed directional radiated power.

In order to be incorporated in the orbit determination process, the results of the Monte Carlo simulations need to be converted in an acceleration fitted by a function of time which can be represented within the ODP (i.e., polynomials up to the fourth order and exponential functions). In such a way, the recoil acceleration is represented by a finite number of parameters and their associated covariance matrix. Since it is reasonable to expect the directionally radiated power, $W_Z = TRF \cdot c$, to be a linear function of the energy input to the system, one can then seek for a regression of the Monte Carlo simulation output of the following kind:

$$W_Z = \boldsymbol{x} \cdot \boldsymbol{P} = x_1 P_{\mathrm{th}} + x_2 P_{\mathrm{el}} + x_3 \tilde{\Phi}_S, \tag{8}$$

where x_i, $i = 1, 2, 3$ are coefficients to be determined. To preserve homogeneous dimensions, a solar power, $\tilde{\Phi}_S$, has been introduced, equal to the solar flux times the projected surface of the high-gain antenna (HGA). This approach is similar to that used by Turyshev *et al.* in Ref. [14], except that here we explicitly account for the solar power contribution in the fit of the thermal simulation.

A least-squares fit of the Monte Carlo results provided the vector of regression coefficients $\boldsymbol{x}$ with associated covariance matrix Γ_x, as shown in Table III.

TABLE III. Regression coefficients for anisotropic IR emission of the Pioneer probes as a function of the on-board power and solar flux.

Estimated $\boldsymbol{x}$	Estimated $\boldsymbol{\sigma}$	Normalized covariance Γ_x		
0.0132	1.76×10^{-4}	1	−0.905	0.195
0.553	8.17×10^{-4}	−0.905	1	−0.478
−0.207	9.02×10^{-3}	0.195	−0.478	1

A total of $n_{\mathrm{sim}} = 1000$ simulations were performed, each using a triplet $(P_{\mathrm{th}}, P_{\mathrm{el}}, \Phi_S)$. The termination criterion used was the invariance of the resulting statistics: the least-squares fit was performed incrementally over the simulations, i.e., using a number of points ranging from 1 to n_{sim}, and the difference between two subsequent fit outputs monitored. The percentage variations of the elements of the regression vector and covariance matrix stabilized within 0.3% after around 500 simulations. As a measure of the scatter of the simulation results, one can look at the post-fit residuals after linear regression, which exhibit a standard deviation of $\simeq$4.5 W, while their mean is $\simeq$0.1 W (to be compared to the magnitude of the anisotropic power, in the order of a few tens of watts). The covariance matrix shown in Table III globally accounts for the uncertainties in the internal distribution of thermal power inside the RTGs and the electrical power inside the spacecraft body, as well as uncertainties in surface optical properties and, finally, the goodness of the assumed linear fitting function for the thermal recoil force. There are, however, other sources of error which may affect the thermal model. First, while the power values are known inputs to the thermal model, their temporal evolution during the trajectory is not perfectly known. Indeed, the telemetry readings from which the thermal and electrical power values are retrieved have limited resolutions: according to Refs. [10,16], the confidence in P_{th}, P_{el} is limited to 2.1 and 1.8 W, respectively, at the 1σ level. Moreover, the solar flux is not a measured quantity, being rather estimated through an approximate relation assuming a decay proportional to the heliocentric distance squared ($\Phi_S = 1366/\mathrm{AU}^2\,\mathrm{W/m}^2$). Its uncertainty was modeled in this study solely in terms of the flux constant at 1 AU, to which a 1σ of ± 4 W was assigned [25]. Inclusion of all these error sources can be accomplished by applying the theory of linear estimation in the presence of consider parameters [26]. The mathematical details will be skipped for the sake of brevity—suffice it to say that the overall result is an additional covariance to be added to the one in Table III.

To integrate the thermal recoil acceleration in the ODP in a consistent manner, one needs to map the representation found in Eq. (8), as a function of power sources, to the time domain. In Ref. [10], plots of thermal power inside RTGs (total expected power minus the telemetered electrical power) and of the electrical power dissipated from instrumentation placed inside the spacecraft body are found. Computation of the solar flux variation over time requires the spacecraft's heliocentric distance, which grows almost linearly in time during the interplanetary cruise: the exact variation is retrieved from orbital solutions for Pioneer 10 and 11 and fitted with a suitable function of time. A combination of polynomials and exponential functions was found to provide a satisfactory fitting of the time evolution of power data, and they are functions natively incorporated in the ODP as acceleration models.

We mentioned above that the IR emission is not the only kind of energy radiated into space by Pioneer, since there is also the power, nominally 8 W, carried by the collimated radio beam transmitted by the high-gain antenna. This aspect is discussed in Ref. [9], where an efficiency of the conversion from power to linear momentum of 0.83 is computed: this value has been used in the present study as well. The resulting force pushes the probe away from the Sun; thus it has to be subtracted from the thermal recoil acceleration just computed. In this way, a global radiation recoil force (RF) expression [27], to be integrated in the orbit analysis discussed hereafter, was computed for Pioneer 10 and 11 as follows:

$$\begin{aligned} a_{RF_{P_{10}}} &= A_{RF} + B_{RF}\tau + C_{RF}\tau^2 + G_{1RF}e^{-\beta_1\tau_1} \\ &\quad + G_{2RF}e^{-\beta_2\tau_2} \\ a_{RF_{P_{11}}} &= A_{RF} + B_{RF}\tau + C_{RF}\tau^2 + A_{\phi_i} + B_{\phi_i}\tau_i + C_{\phi_i}\tau_i{}^2 \\ &\quad + D_{\phi_i}\tau_i{}^3 + E_{\phi_i}\tau_i{}^4, \quad i = 1, 2. \end{aligned} \tag{9}$$

In the above equation, the first three terms account for the on-board power contribution to radiation force, while the remaining (exponentials for Pioneer 10, fourth-order polynomials for Pioneer 11) account for the solar flux; $\tau =$ seconds past launch; $\tau_1 =$ seconds past 1 September 1977, up to τ_2; $\tau_2 =$ seconds past 12 September 1980. In the expression applicable to Pioneer 11, two fourth-order polynomials have been used for fitting the two segments of trajectory covered by tracking data, prior to and after the Saturn encounter. For convenience, we can collect the coefficients of the recoil force in a vector $\boldsymbol{\xi}_{P10} = [A_{RF}\ B_{RF}\ C_{RF}\ G_{1RF}\ G_{2RF}]$ for Pioneer 10, and in an analogous $\boldsymbol{\xi}_{P11}$ for Pioneer 11.

Mapping of the covariance matrix from power coefficients, Γ_x, to force coefficients, Γ_ξ, can be accomplished via an orthogonal transformation, i.e. a change of coordinates $\boldsymbol{x} \to \boldsymbol{\xi}(\boldsymbol{x})$. One last source of uncertainty is introduced when computing the thermal recoil acceleration starting from the corresponding force, since the mass of the spacecraft is not exactly known. Again, an additional covariance can be computed using an orthogonal transformation, so that the total covariance of the acceleration coefficients, Γ_{RA}, can be found as

$$\Gamma_{RA} = \frac{1}{m_0^2}\Gamma_{RF} + \frac{\sigma_m^2}{m_0^4}\boldsymbol{\xi}\boldsymbol{\xi}^T, \tag{10}$$

where σ_m is the mass uncertainty assumed to be equal to 9 kg and the nominal mass m_0 is set equal to 246.4 and 235.9 kg for Pioneer 10 and Pioneer 11, respectively (see discussion in Sec. III). The graphical representation of the curves in Eq. (9) are shown in Fig. 4 for both Pioneers 10 and 11; as an example, the numerical coefficients, together

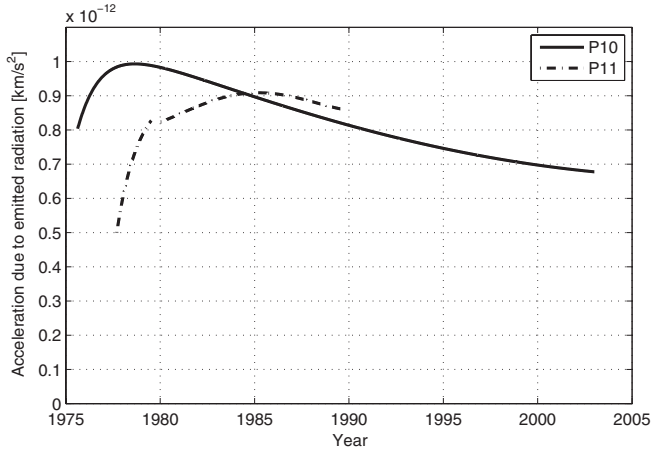

FIG. 4. Acceleration due to emitted radiation by Pioneer 10 (full line) and Pioneer 11 (dash-dotted line) along the trajectory segments covered by the analyzed tracking data. The gap in the Pioneer 11 curve around 1979 corresponds to the Saturn encounter.

with the mapped 1σ uncertainties for Pioneer 10 radiation recoil acceleration, are collected in Table IV.

The curves in Fig. 4 show clearly that the radiation acceleration undergoes a significant temporal variation: indeed, by looking from left to right we first see that TRA increases due to the vanishing (outward) contribution of the solar flux. Later, at sufficiently high heliocentric distances, the (Sunward) contributions from the RTGs' heat reflected by the antenna back side and the heat rejected by the louver system become dominant and exhibit the expected decrease due to radioactive decay of the nuclear fuel. We point out that the maximum recoil acceleration occurs for Pioneer 10 at $\simeq 16$ AU, while for Pioneer 11 it occurs at $\simeq 19$ AU. The maximum value acting on Pioneer 11 is lower than that of its predecessor, since the former resided longer within the Solar System due to a second planetary encounter at Saturn. Hence, Pioneer 11 reached distances where the effect of solar flux was negligible later in its operational life, when the available on-board power had already significantly decreased.

TABLE IV. Fitting coefficients of Pioneer 10 recoil acceleration as a function of time.

Coefficients	Estimated value	1σ
A_{RA} [km/s^2]	1.246×10^{-12}	5.49×10^{-14}
B_{RA} [km/s^3]	-9.911×10^{-22}	4.22×10^{-23}
C_{RA} [km/s^4]	4.191×10^{-31}	1.81×10^{-32}
G_{1RA} [km/s^2]	-2.685×10^{-13}	1.62×10^{-14}
G_{2RA} [km/s^2]	-7.148×10^{-13}	4.31×10^{-15}
β_1 [1/s]	-7.148×10^{-13}	…[a]
β_2 [1/s]	-7.148×10^{-13}	…

[a]No uncertainties are given to the exponential frequency factors, since they represent the mapping of the $1/r^2$ term of the solar flux, which was assumed to be unaffected by errors.

III. TRACKING DATA ANALYSES

Two sets of Doppler tracking data have been analyzed during this study, which cover the time intervals from 13 February 1980 to 2 March 2002 for Pioneer 10 and from 1 November 1977 to 30 September 1990 for Pioneer 11, using NASA-JPL's Orbit Determination Program (ODP). This code includes a model of the Solar System dynamics to compute spacecraft trajectories. Based on the computed trajectory, it further calculates the predicted radio tracking observables (the so-called computed observables) between the ground stations and the spacecraft. The difference between the observed and the computed observables (the so-called residuals) is then fed to a recursive filter in order to improve the knowledge of a certain set of parameters affecting the spacecraft dynamics (estimated parameters). Such parameters include, as a minimum, the spacecraft state vector at a certain epoch; other parameters may be the mass and gravity field of celestial bodies, their orbits and orientation parameters, or other quantities of interest for navigation and science. Previous orbital solutions for Pioneer 10 and 11 required the addition of a Sunward acceleration of unknown origin to those computed using the implemented dynamical models, both of gravitational and nongravitational origin, in order to obtain zero-mean residuals. Such additional acceleration has become known as the Pioneer Anomaly, and lacking its inclusion, the Doppler residuals show an almost constant drift of 0.4 Hz/year, corresponding to an unmodeled acceleration of $\approx 8.5 \times 10^{-13}$ km/s^2. The trajectory reconstruction is performed in the ODP by integrating the equations of motion, expressed in terms of the total acceleration acting on the spacecraft. The gravitational forces include central-body and secondary-body Keplerian point mass accelerations, higher-order gravity harmonics, and relativistic effects. Of course, not all of these contributions are always relevant for the trajectory under study.

A. Nongravitational accelerations

Relevant nongravitational accelerations during Pioneer's interplanetary cruise arise from the solar radiation pressure and propulsive maneuvers, plus, as shown in Sec. III, the acceleration due to radiation nonisotropically emitted. The former is included as a dynamical model in the ODP in which the spacecraft parts are represented by a series of geometric entities (parabolic antenna, boxes, flat plates, spheres and cylinders). The momentum exchange between the photons and each component is computed as a function of its specular and diffuse reflection coefficients, and summed up. Because of the geometrical configuration of the Pioneers, having a big antenna dish constantly directed towards the Earth, the only component significantly

contributing to the solar pressure is the antenna itself, which is almost always in a full front illumination condition [28]. Using a simplified flat plate model, one can compute the following expression for the solar radiation pressure [29]:

$$a_{\mathrm{SRP}} = \frac{1 + 2(\mu_F + \nu_F)\cos(\vartheta)}{c \cdot m} \frac{A \Phi_{S@1}}{d^2}, \qquad (11)$$

where μ_F and ν_F are the specular and diffuse reflective coefficients of the HGA's Earth-facing side, which are assumed to be constant (i.e., the degradation factors have been neglected), A is its area, m is the spacecraft mass, $\Phi_{S@1}$ is solar flux at 1 AU, and ϑ is the angle between the direction of the Sun and the HGA axis. Nominal values for μ_F and ν_F coming from JPL calibration at early stages in the mission are 8.055×10^{-2}, 2.757×10^{-1} for Pioneer 10 and 7.016×10^{-2}, 2.808×10^{-1} for Pioneer 11. However, as reported in Ref. [17], determination of these coefficients from the solar acceleration inferred from tracking data may be affected by errors in the spacecraft mass, which is not exactly known. Equation (11) can be exploited to compare the relative magnitudes of the solar radiation pressure and the thermal recoil acceleration along the spacecraft trajectories. In Fig. 5, these quantities are plotted for Pioneer 10 and 11 for the time periods covered by the available tracking data. The relative magnitudes are quite different for the two spacecraft: Pioneer 10 has a solar radiation pressure acceleration which is almost always smaller than the thermal recoil, even negligible for a large part of the trajectory. On the contrary, during Pioneer 11's route from Jupiter to Saturn, the solar radiation pressure is roughly 1 order of magnitude higher than the thermal recoil, while in the later stages of the cruise the two nongravitational accelerations are comparable. This different dynamics has an impact on the observability of the anomalous acceleration using tracking data, as will be discussed later in Sec. IV A.

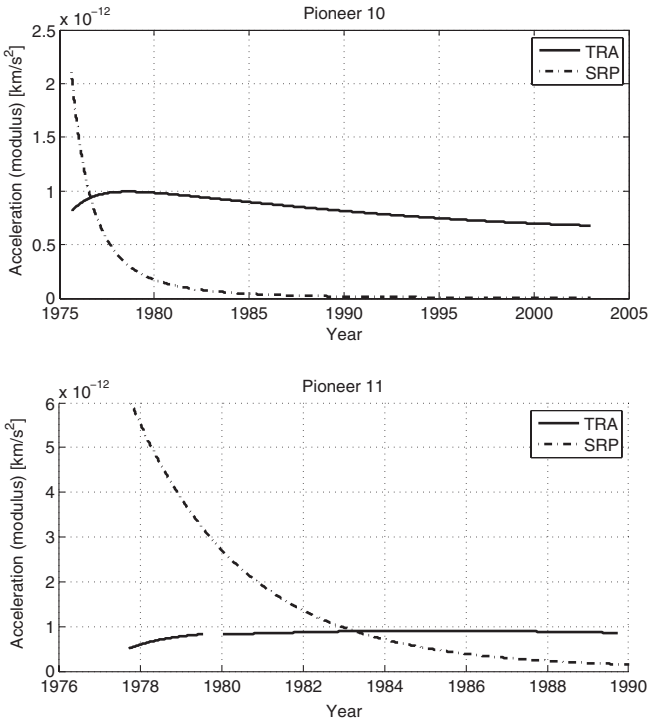

FIG. 5. Comparison between the magnitude of the RA (solid) and the SRP (dashed) for Pioneer 10 (top panel) and 11 (bottom panel).

As far as propulsive forces are concerned, the hydrazine thrusters on board the spacecraft were aimed at three types of maneuvers: precession maneuvers, i.e. HGA repointing towards the Earth to guarantee communication link; delta-V maneuvers for trajectory control; and spin/despin maneuvers. After the planetary encounters, only precession maneuvers were performed (more than 100 in the time period covered by the analyzed data sets). Even if the precession maneuvers are expected to exert only torques on the spacecraft and no net forces, possible thruster malfunctioning, due for example to asynchronous operation of thrusters or valve leaks, may have given rise to small residual forces. The times at which maneuvers were executed are available through telemetry, together with the records of the commanded thruster pulses. From these data, however, it is not possible to infer the magnitude of the (unintended) velocity increments possibly produced during maneuvers. Rather, the only means of estimating such velocity increments is using the radiometric data, i.e. to treat them as parameters to be estimated in the orbit determination analysis and check if such parameters are actually observable and/or they improve the overall quality of the fitting. This was the case for all the precession maneuvers analyzed in this study.

Nongravitational accelerations are mass dependent, therefore the spacecraft mass must be provided as an input. The Pioneers' masses were nearly 259 kg (223 kg of dry mass plus 36 kg of propellant) at launch, and this value was expected to decrease along the course of the mission because of propellant consumption. However, the mass was not telemetered, and its value after the planetary encounters could only be reconstructed approximately. In Refs. [17] and [16], reference values for Pioneer 10 mass are 241 and 251.8 kg, while for Pioneer 11 the reported figures are 232 and 239.7 kg. In the present study, the average values of 246.4 and 235.9 kg were used as nominal masses for Pioneer 10 and 11, respectively. The uncertainty associated with these values was set to 9 kg, around one quarter of the propellant mass [17], and was accounted for in the computation of the TRA as an additional covariance for the polynomial coefficients (see discussion in Sec. II C).

B. Media calibrations

The ODP implements accurate models to account for media and antenna corrections to the propagation of

tracking signals. Media corrections consists of corrections due to the Earth's troposphere and corrections due to charged particles which can be in the Earth's ionosphere, in space (interplanetary plasma), or in the solar corona [30]. The delay due to the solar corona is computed by a built-in ODP model (see Ref. [30] and references therein), while other effects can be accounted for if the user provides as input the zenith path delay in the form of polynomials or Fourier series coefficients. In this study, tropospheric effects have been included in the form of seasonal corrections for the dry and wet delay, while corrections for ionosphere path delays based on Klobuchar's work [31] were initially included but then disregarded since they did not provide a substantial improvement to the orbital fit. The ODP further includes the possibility of correcting the computed residuals for any other possible phenomenon affecting them. An example directly applicable to the Pioneers is the data calibration to account for the Doppler shift induced by the spacecraft spin rate (the so-called Marini's effect).

C. Implementation techniques for the orbital analyses

The data analysis using the ODP was aimed at obtaining satisfactory orbital solutions incorporating the recoil acceleration, possibly without adding any other unknown acceleration. Even if the computed recoil accelerations shown in Fig. 4 are time varying in contrast with the acceleration reported as constant in Ref. [17], or decreasing monotonically [16], one should keep in mind that the measured unknown acceleration is actually a Doppler shift in the radiometric data, while the reported solutions for accelerations are just one way to obtain good orbital solution (i.e., a satisfactory fit of tracking data). Other orbital solutions may be investigated, based on dynamical models which differ from one single constant acceleration, and possibly relying on a physical basis. Indeed, the thermal analysis presented in Sec. II provides one such model.

The implementation of the orbital analyses presented relied on two different filtering techniques, which are discussed in the following.

In principle, the trajectory followed by a spacecraft, independently from its time length, can always be fitted by a single orbital arc function of the initial spacecraft state vector, plus that of every other parameter which affects its dynamics. It is therefore reasonable to include all tracking data available for a certain spacecraft into a single-arc analysis, so that all the observables contribute to the orbit determination. On the other hand, the complexity of the physics underlying certain spacecraft dynamics, especially in the presence of extremely long arcs, makes it highly improbable that the trajectory can be perfectly represented by a single deterministic model; thus, in practice, one must deal with a certain degree of model deficiency.

The Pioneers' tracking data, lasting more than a decade, are likely to be prone to such a problem. To overcome these difficulties, one may exploit the use of a dynamic compensation through multi-arc filtering, which has been widely used in the Cassini spacecraft's scientific investigation [32–34]. With this method, orbital fits are obtained from shorter data arcs (from 6 months to 1 year in the present study). In the multi-arc technique, the set of estimated parameters is separated into two groups: global parameters, common to all arcs, and local ones, which affect only the arc to which they belong.

For the Pioneers, the parameters which may be treated as local, other than initial-state vectors, are the maneuvers' velocity increments; the "anomalous" acceleration is set as a global parameter so that all the available tracking data concur to its estimate. For each trajectory arc, the orbit determination steps are performed independently, up to the computation of the observation residuals and their partial derivatives with respect to the local and global parameters. These are then combined to allow their processing by the estimation filter. The start and end times for each arc were set at maneuver occurrences; this way, there is a certain similarity with the single-arc approach, as both allow for trajectory discontinuities at maneuvers: the former allows for instantaneous velocity increment, while the multi-arc allows for both velocity and position increments.

The *a priori* state vector components at the beginning of each arc were generated by mapping the single-arc orbital solution to the epochs of interest. Their *a priori* uncertainties were set equal to 10 times the *a posteriori* uncertainty from the single-arc solution for the position vector; on the contrary, the uncertainty of the velocity components were kept completely unconstrained to allow for a correct maneuver estimate. For the single-arc analysis, the parameters to be estimated are the initial-state vector

TABLE V. Parameters treated as consider with their *a priori* uncertainty (the nomenclature follows the ODP syntax; see footnote for explanations).

Parameter	*A priori* sigma
MUF[a]	0.015
NUF	0.056
CORONA	4×10^3 m
CORONB	1.8×10^2 m
CORONC	0.8×10^6 m
TROPDj	5×10^{-2} m
TROPWj	1×10^{-1} m
LOii	1.57×10^{-5} deg
CVii	1×10^{-1} m
CUii	1×10^{-1} m

[a]MUF, NUF $= \mu_F, \nu_F$ coefficients of HGA Earth-pointing side; CORONA, CORONB, CORONC = characteristics constants for the solar corona path delay model; TROPODj, TROPOWj = constant bias to the tropospheric zenith dry and wet path delays at DSN Complex j; LOii, CVii, CUii = longitude, height above equator and spin axis distance of Earth station ii.

components, the velocity increments due to maneuvers and a constant acceleration, consistently with the multi-arc approach. From an implementation point of view, the standard single-arc filter is just a special case of the more general multi-arc filter.

Other parameters were added as consider, and their uncertainty was accounted for in the computation of the formal error of the estimated parameters (see Sec. V): these include the HGA reflective coefficients for SRP computation, the solar corona parameters, the tropospheric zenith path delay, and the Earth station locations.

Doppler data were edited including spin compensation, data rejection and data weighting. Spin compensation was carried out according to Ref. [35]. For the present analyses, data were rejected when tracking from an elevation angle lower than 20 deg. Furthermore, clear outliers and biased points were manually detected and deleted. Doppler observables were weighted in the least-square estimation filter according to the standard deviation of their residuals computed on homogeneous sets of data. To this aim, an automatic routine for data weight assignment was implemented: this allowed the post-fit sum of squares to be slightly lower than the number of observables, thus avoiding data overweighting.

IV. RESULTS

A. Reestimating the unknown acceleration

The first analysis performed consisted of reestimating a constant acceleration using the extended data set of Pioneer 10 and 11, without accounting for the output of the thermal model discussed in Sec. II, using both the single-arc and the multi-arc approaches (see Table VI). The formal uncertainties of the estimated accelerations are reported for all test cases, along with the corresponding values when including the consider parameters written between round brackets. This first test group is identified with the number 1, followed by an indicator of the spacecraft (P10 or P11) and the filter (SA, MA). For Pioneer 10, both single-arc and multi-arc techniques were used (first two rows in Table VI). For the MA, 46 arcs were implemented, each bounded in between two maneuvers and lasting approximately 6 months. For Pioneer 11, there are two well-separated trajectory segments, the first encompassing the Jupiter-to-Saturn transfer orbit and a longer data set for the post-Saturn encounter trajectory. These have been treated as single arcs (rows 3 and 4 in Table VI), and as the combination of two arcs (labeled with 2A to indicate a multi-arc with only two arcs), but also as a set of multiple arcs. Indeed, due to the very large number of maneuvers, it would have been unpractical to create one arc between each couple of maneuvers; moreover, it should be noted that the MA dynamic compensation has been motivated mainly by the evidence of periodic signatures of half a year in the residuals [36] and the annual oscillatory term in the acceleration [17], which indicate the time scale at which modeling errors become significant. We thus used for Pioneer 11 a total of 11 arcs lasting approximately one year, each of them having a number of maneuvers treated as local parameters.

TABLE VI. Summary of Test Set 1 with estimation of a constant acceleration, TRA not included. Acceleration uncertainties including the consider parameters are reported in round brackets.

Test case	Post-fit residuals		Acceleration
	μ [mHz]	σ [mHz]	$[\mathrm{km/s^2}] \times 10^{-13}$
1.P10/SA	−0.01	3.8	$8.18 \pm 0.01\ (0.08)$
1.P10/MA	−0.02	3.3	$7.90 \pm 0.05\ (0.06)$
1.P11-preS[a]/SA	−0.10	4.3	$0.89 \pm 0.60\ (4.40)$
1.P11-postS[b]/SA	−0.06	14.1	$7.61 \pm 0.16\ (0.52)$
1.P11/2A	−0.07	13.4	$7.06 \pm 0.15(0.76)$
1.P11/MA	−0.06	13.4	$7.15 \pm 0.19(0.82)$

[a]prior to the Saturn encounter.
[b]after the Saturn encounter.

The different orbital solutions obtained are compared in terms of their mean (μ) and standard deviation (σ) of the residuals and shown in Table VI. As a general trend, satisfactory orbital solutions are obtained in all cases, with some advantages in terms of lower residuals' standard deviation when using overparameterization through the multi-arc approach. As an example, plots of Doppler residuals for the whole time span covered by the available tracking data are shown in Figs. 6 and 7 for Pioneers 10 and 11, respectively.

The estimated acceleration values obtained from these preliminary test cases are quite similar to those of other references. It should be noticed that Pioneer 10 post-fit residuals exhibit lower standard deviation levels than their Pioneer 11 counterparts. As for the pre-Saturn encounter

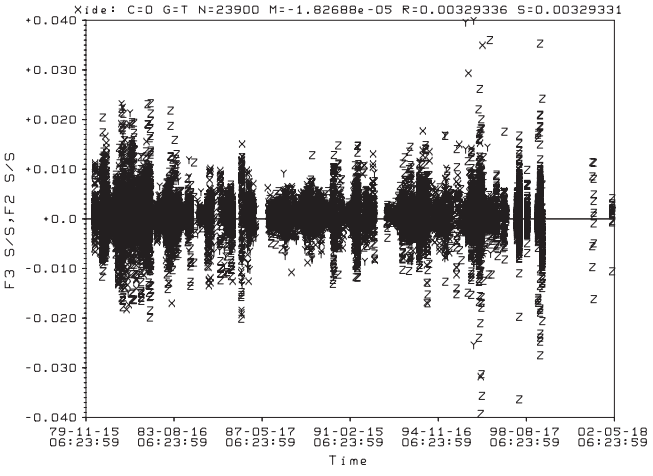

FIG. 6. Post-fit residuals obtained for Pioneer 10 after estimating for a constant acceleration, corresponding to test case 1.P10/MA of Table VI.

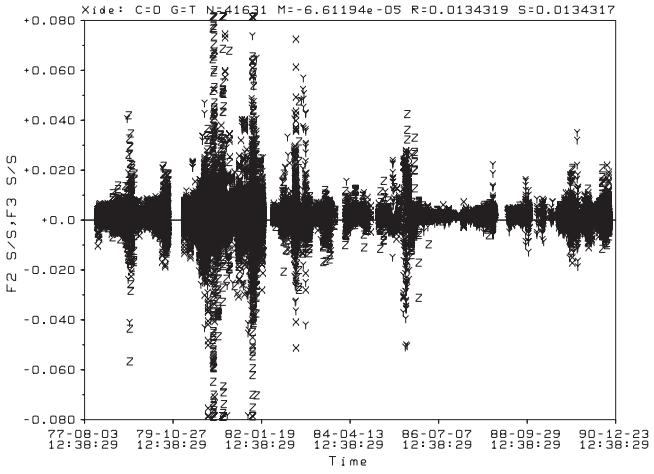

FIG. 7. Post-fit residuals obtained for Pioneer 11 after estimating for a constant acceleration, corresponding to test case 1.P11/2A of Table VI.

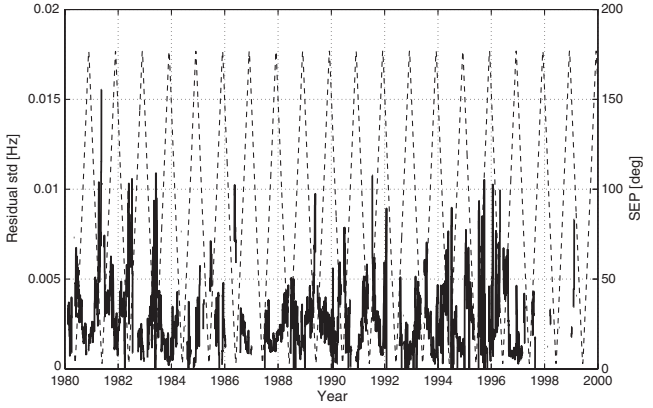

FIG. 8. Standard deviation of Pioneer 10 post-fit residuals calculated over 15-day batches (full line) and SEP angle variation (dashed line) from 1980 to 2000.

data of Pioneer 11, the value of the acceleration is statistically null, in agreement with what is reported in Ref. [11]. This result is not surprising, as in this part of the trajectory the solar radiation pressure is dominant with respect to the acceleration of thermal origin (see bottom panel of Fig. 5). In general, tracking data of Pioneer 11 cover heliocentric distances at which the solar pressure is larger than, or at least comparable to, the thermal recoil acceleration. Indeed, if we add μ_F and ν_F as solve-for parameters, the resulting acceleration varies considerably. This is an indication that the actual magnitude of the anomalous acceleration is correlated with the solar pressure, or equivalently, a portion of the anomalous acceleration may be due to errors in the modeling of solar radiation pressure. The first segment of Pioneer 11's trajectory is subjected to this to an even higher extent: by looking at the acceleration uncertainty of test case 1.P11-preS/SA, it is clear how an acceleration of order of magnitude 10^{-12} km/s^2 or less is hardly, if not at all, observable. Furthermore, it can be noticed that the overparametrization has a beneficial effect on the quality of the orbital solution of Pioneer 10, when looking at the residuals' standard deviation, which lowers from 3.7 to 3.3 mHz. The reduction of the residuals' standard deviation comes at the expense of a loss of formal accuracy (increase in the consider sigma) of the estimated acceleration; this is a well-known effect in estimation filters when the number of solve-for parameters is increased without injecting additional information from other observations.

As mentioned in Sec. III C, previous studies highlighted the presence of periodic signatures in post-fit residuals, and an annual modulation of the anomalous acceleration when estimated as a stochastic process. These conclusions were drawn from analysis of the early data set made available for Pioneer 10 (1987–1998). In the present work, the periodic modulation of the anomaly has been addressed as well, this time over the entire extended data set of Pioneer 10, but at a mainly qualitative level. Since S-band Doppler data are known to be highly sensitive to dispersive noise sources, a likely cause of such periodic signatures is the uncompensated delay due to the charged particles found in the solar plasma and Earth ionosphere. As previously mentioned, the ODP includes a model for solar plasma compensation; however, while such a model is expected to perform satisfactorily when applied to range data, on the contrary, it performs quite poorly for Doppler data [37]. We tested the possible correlation between the goodness of residuals and the solar plasma by comparing the temporal evolution of the standard deviation of post-fit residuals batches lasting 15 days, along with the Sun-Earth-probe (SEP) angle. The outcome is shown in Fig. 8, where several standard deviation peaks are found in correspondence to low SEP angles. Starting from this evidence, it is quite natural that any spectral analysis of the residuals may highlight annual peaks; at the same time, given the periodic modulation of the Doppler signal, an acceleration with the same frequency can compensate for it, improving the data fit: the previously reported results [17], in this respect, are hence of no surprise. Summarizing, the authors are firmly convinced that the temporal modulation of the anomaly is an artifact due to imperfect media calibration—in particular, solar plasma: as a consequence, this issue has not been the object of further investigation.

B. Orbital solutions including the recoil force

The preliminary orbit analyses summarized in Table VI have been repeated with the following variants:

1. Test Set 2, where the TRA model is included in the trajectory reconstruction and treated as consider.
2. Test Set 3, where TRA is included as consider and an additional bias acceleration is estimated (global parameter in the case of multi-arc). This is an original contribution of the present study, which has not been reported in Ref. [14].

TABLE VII. Summary of Test Set 2, including TRA, with no additional acceleration estimated.

Test case	Post-fit residuals	
	μ [mHz]	σ [mHz]
2.P10/SA	−0.02	3.6
2.P10/MA	−0.02	3.3
2.P11-preS/SA	−0.12	4.4
2.P11-postS/SA	−0.06	14.1
2.P11/2A	−0.07	13.4
2.P11/MA	−0.06	13.4

TABLE VIII. Summary of Test Set 3, including TRA and the estimation of an additional constant acceleration (acceleration uncertainties in the presence of consider parameters reported in round brackets).

Test case	Post-fit residuals		Acceleration
	μ [mHz]	σ [mHz]	[km/s^3]
3.P10/SA	−0.03	3.6	$0.18 \pm 0.01(0.44)$
3.P10/MA	−0.02	3.3	$0.83 \pm 0.05(0.52)$
3.P11-postS/SA	−0.06	14.1	$-1.12 \pm 0.12(0.67)$
3.P11/2A	−0.06	13.4	$-1.62 \pm 0.15(0.87)$
3.P11/MA	−0.06	13.4	$-1.35 \pm 0.19(0.92)$

The introduction of an additional acceleration for Test Set 3 has the purpose of checking whether thermal recoil force is enough to explain the whole anomaly, or if a residual unmodeled acceleration still provides an improved orbital solution. The parameters which are treated as consider are those listed in Table V plus the coefficients for the recoil acceleration. Results are summarized in Tables VII and VIII and discussed afterwards; sample plots of post-fit residuals obtained, including recoil accelerations for the Pioneer 10 and 11 complete data sets, are shown in Figs. 9 and 10. Since the acceleration in the pre-Saturn encounter of Pioneer 11 is unobservable, the case 3.P11-preS is not reported in Table VIII. When including time-varying accelerations according to our thermal model, orbital solutions are obtained for Pioneer 10 and for the two segments of Pioneer 11, without adding any other acceleration. This is an implicit confirmation that the observed drift in the Doppler residuals is compatible with time-varying acceleration. The quality of the fit is equivalent to that of the solutions obtained with Test Set 1, as emerges by comparing Figs. 6 and 7 with the corresponding Figs. 9 and 10, as well as the post-fit residual statistics in Tables VII and VIII. In particular, in the residuals displayed in Figs. 9 and 10, no drift or signatures are present which might indicate any residual unaccounted acceleration. A confirmation of this is found with Test Set 3: the additional acceleration cannot be clearly estimated, since the estimated value is not sufficiently larger than its consider sigma, this being especially true for Pioneer 10 (lower bias-to-sigma ratios). Most importantly, even when the acceleration is larger than 2σ, there is absolutely no gain in the orbital solution quality by the introduction of this additional term. All the above considerations hold for both Pioneer 10 and 11, as well as for single-arc and multi-arc filtering. In summary, all simulations performed lead to the same conclusion: there is no anomalous acceleration acting on Pioneer 10 and 11. The reported unexplained drift in Doppler residuals disappears when including the force due to anisotropic radiation emission into the dynamical model of the probes.

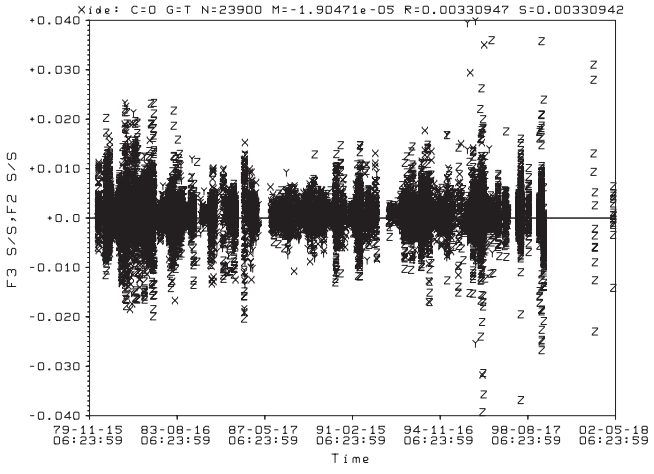

FIG. 9. Post-fit residuals obtained for Pioneer 10, after including the recoil force dynamical model, corresponding to test case 2.P10/MA of Table VII.

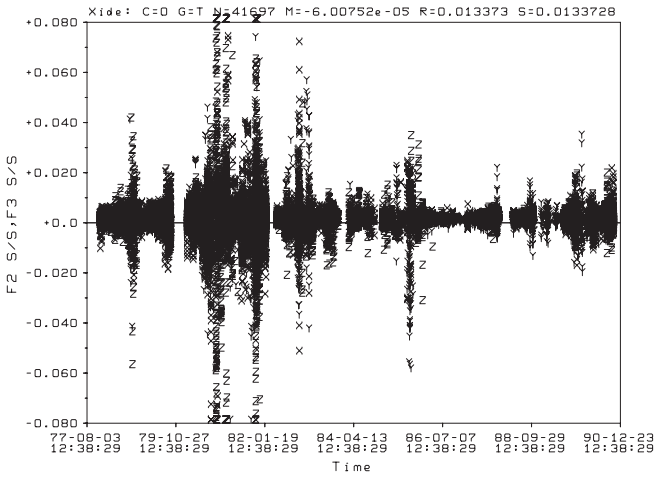

FIG. 10. Post-fit residuals obtained for Pioneer 11, after including the recoil force dynamical model, corresponding to test case 2.P11/MA of Table VII.

V. CONCLUSIONS

Orbital solutions for Pioneer 10 and 11 spacecraft using the available radiometric observables were presented. The data processing was carried out, taking into account the results of a thermal model of the spacecraft aimed at

evaluating the recoil force due to anisotropic radiation. The thermal model includes the main spacecraft components and was built using the available design documentation. Monte Carlo simulations allowed us to perform a sensitivity analysis on the solution, and to represent the thermal acceleration along the trajectory using a finite number of parameters and their associated uncertainties. Such representation is suitable of being incorporated in the orbit determination process in a consistent manner.

Processing of radiometric data was performed using the NASA/JPL's ODP. Both single-arc and multi-arc estimation techniques were implemented, and the resulting orbital solutions thoroughly compared. The multi-arc technique provides a means to compensate for deficiencies in dynamical models when the trajectory arc is extended in time, allowing for a slightly better quality of the post-fit residuals. The systematic estimation of velocity increments due to each propulsion maneuver was also included as a necessary step to reach a good orbital solution.

Our results show that the computed thermal recoil acceleration, though not constant in time, is the only factor responsible for the observed linear drift in the Pioneer Doppler data, consistent with what is reported in Refs. [12–14]. Our orbital solutions were obtained without the need for any empirical acceleration in addition to the thermal recoil one. We also tried including the estimation of an additional constant acceleration, but it did not improve the quality of the orbital fits; moreover, its estimated value is statistically compatible with zero. All these results lead to the conclusion that no anomalous acceleration acted on the Pioneer 10 and 11 spacecraft along their interplanetary trajectories, once all systematic effects, and in particular the thermal recoil force, are included in the dynamical model: the Pioneers follow trajectories which are fully compatible with the Newton-Einstein laws of gravity.

ACKNOWLEDGMENTS

The authors are grateful to Slava G. Turyshev for his survey on the Pioneer investigation status, Victor T. Toth for his advice on telemetry data, and Ruaraidh Mackenzie for his valuable hints on multi-arc analysis. The work of D. M. and P. T. has been funded in part by ASI (Agenzia Spaziale Italiana).

[1] J. D. Anderson, P. A. Laing, E. L. Lau, A. S. Liu, M. M. Nieto, and S. G. Turyshev, Phys. Rev. Lett. **81**, 2858 (1998).
[2] C. B. Markwardt, arXiv:gr-qc/0208046.
[3] V. T. Toth, Int. J. Mod. Phys. D **18**, 717 (2009).
[4] B. Levy, A. Christophe, P. C. J. M. Metris, G. Brio, and S. Reynaud, Space Sci. Rev. **151**, 105 (2010).
[5] S. Reynaud and M. Jaekel, arXiv:0801.3407v1.
[6] J. R. Brownstein and J. W. Moffat, Classical Quantum Gravity **23**, 3427 (2006).
[7] J. I. Katz, Phys. Rev. Lett. **83**, 1892 (1999).
[8] J. D. Anderson, P. A. Laing, E. L. Lau, A. S. Liu, M. M. Nieto, and S. G. Turyshev, Phys. Rev. Lett. **83**, 1893 (1999).
[9] L. K. Scheffer, Phys. Rev. D **67**, 084021 (2003).
[10] V. T. Toth and S. G. Turyshev, Phys. Rev. D **79**, 043011 (2009).
[11] S. G. Turyshev, V. T. Toth, J. Ellis, and C. B. Markwardt, Phys. Rev. Lett. **107**, 081103 (2011).
[12] F. Francisco, O. Bertolami, P. Gil, and J. Pramos, Phys. Lett. B **711**, 337 (2012).
[13] B. Rievers and C. Lämmerzahl, Ann. Phys. (Berlin) **523**, 439 (2011).
[14] S. G. Turyshev, V. T. Toth, G. Kinsella, S.-C. Lee, S. M. Lok, and J. Ellis, Phys. Rev. Lett. **108**, 241101 (2012).
[15] TRW Systems Group, Technical Report, "Pioneer F/G Spacecraft Operational Characteristics PC-202", NASA Ames Research Center.
[16] S. G. Turyshev and V. T. Toth, Living Rev. Relativity **13**, 4 (2010).
[17] J. D. Anderson, P. A. Laing, E. L. Lau, A. S. Liu, M. M. Nieto, and S. G. Turyshev, Phys. Rev. D **65**, 082004 (2002).
[18] Averaged over all directions and wavelengths of radiation.
[19] M. F. Modest, *Radiative Heat Transfer* (Academic Press, New York, 2003), 2nd ed.
[20] A Lambertian emitter is a surface for which the directional radiative flux (energy flow per unit angle per unit surface area) is proportional to the cosine of the polar angle [19]. A Lambertian reflector may be defined in an analogous manner. The gray assumption further implies that reflectance ρ equals $1-\varepsilon$.
[21] Usually the effect on the emittance is small, unless severe deposition of dust occurs such to sensibly modify the surface coating [22].
[22] G. D. Gilmore, *Spacecraft Thermal Control Handbook* (Aerospace Corporation, El Segundo, CA, 2002), 2nd ed.
[23] $Q_{\rm el}$ and $Q_{\rm th}$ are volumetric heat coefficients related to the total thermal and electrical powers as follows:

$$P_{\rm th}=\iiint_{\rm RTGs} Q_{\rm th}\,dV_R, \qquad P_{\rm el}=\iiint_{\rm Bus} Q_{\rm el}\,dV_B.$$

[24] D. Modenini, Ph. D. thesis, University of Bologna, 2012.
[25] The periodic solar cycle induces a variation on the irradiance measured at the Earth's upper atmosphere of about 2 W (http://glory.gsfc.nasa.gov/overview-tsi.html). This number has been conservatively doubled so as to compensate for the inaccuracy of the assumed quadratic decay.
[26] T. Moyer, *Mathematical Formulation of the Double-Precision Orbit Determination Program (DPODP)*, (Jet Propulsion Laboratory, Pasadena, 1971).

[27] In the following, for the sake of simplicity, we will continue to use the expression "thermal recoil force," keeping in mind that the recoil due to the transmitted radio-beam power is also included.

[28] At the heliocentric distances of interest for the analyzed trajectory arcs, the Earth-pointing and Sun-pointing directions are almost coincident as seen by the probes.

[29] Jet Propulsion Laboratory Navigation Software Group, DPTRAJ-DP Users Reference Manual, Volume 1 (1996).

[30] T. D. Moyer, *Formulation for Observed and Computed Values of Deep Space Network Data Types for Navigation*, Deep Space Communications and Navigation Series (Deep Space Communications and Navigation Systems Center of Excellence, Jet Propulsion Laboratory, Pasadena, 2003).

[31] J. A. Klobuchar, Report No. AFCRL-TR-75-0502 (Hanscom Air Force Base, Massachussets, 1975).

[32] L. Iess *et al.*, Science **344**, 78 (2014).

[33] L. Iess, R. A. Jacobson, M. Ducci, D. J. Stevenson, J. I. Lunine, J. W. Armstrong, S. W. Asmar, P. Racioppa, N. J. Rappaport, and P. Tortora, Science **337**, 457 (2012).

[34] L. Iess, N. J. Rappaport, R. A. Jacobson, P. Racioppa, D. J. Stevenson, P. Tortora, J. W. Armstrong, and S. W. Asmar, Science **327**, 1367 (2010).

[35] The total spin-induced shift accounting for the phase cycles added to the uplink and downlink signals is $(1+\alpha_{S/S})f_{\mathrm{SPIN}}$, where f_{SPIN} is the spin frequency of the spacecraft and $\alpha_{S/S}$ is the transponder turnaround ratio, which for an S/S band uplink/downlink configuration is equal to $240/221$.

[36] J.-M. Courty, A. Levy, B. Christophe, and S. Reynaud, Space Sci. Rev. **151**, 93 (2010).

[37] An empirical support to this argument comes from the fact that the orbital solutions remain practically unchanged whether the solar plasma model is included or not.